Tailored Conformational Changes of Dibenzocycloocta-1,5-dienes by Arene Substituent Effects for Controlled Switching

Wenxin Fu<sup>1</sup>, Jiachen Li<sup>3</sup>, Jacqueline Bustamante<sup>1</sup>, Thanh Lien<sup>4</sup>, Ralph W. Adams<sup>5</sup>, Simon J. Teat<sup>6</sup>, Benjamin J. Stokes<sup>4</sup>, Todd M. Alam<sup>7</sup>, Weitao Yang<sup>3</sup>, Yi Liu<sup>2</sup>, Jennifer Q. Lu<sup>1,\*</sup>

<sup>1</sup>Materials Science and Engineering, School of Engineering, University of California, Merced, 5200 North Lake Road, Merced, California 95343, USA. \*Email: <u>ilu5@ucmerced.edu</u>

<sup>2</sup>The Molecular Foundry, Lawrence Berkeley National Laboratory, One Cyclotron Road, Berkeley, California 94720, United States

<sup>3</sup>Department of Chemistry and Department of Physics, Duke University, Durham, North Carolina 27708, USA

<sup>4</sup>Department of Chemistry & Chemical Biology, University of California, Merced, 5200 North Lake Road, Merced, California 95343, USA

<sup>5</sup>School of Chemistry, The University of Manchester, Oxford Road, Manchester M13 9PL, United Kingdom

<sup>6</sup>Advanced Light Source, Lawrence Berkeley National Laboratory, Berkeley, California 94720, United States

<sup>7</sup>Department of Organic Sciences, Sandia National Laboratories, Albuquerque, NM 87185

#### **Abstract**

The conformational change of dibenzocycloocta-1,5-dienes (DBCODs), a rigid-flexible-rigid organic moiety, mimics that of biological systems and lends itself to low-energy switching. The activation energy for upconverting "Boat" to "Chair" conformation of the cyclooctadiene ring is just around 40 kJ/mol. In contrast, the activation energies for upconverting of unsaturated small organic molecular switches, e.g., azobenzenes, are at least 150 kJ/mol and sometimes greater than 250 kJ/mol. Experimental data corroborated with computational calculations have shown that intramolecular hydrogen bond formed by 1, 10 diamide substituents, yielded an activation energy of 70 kJ/mol and raising the temperature at which "Boat" readily converts to "Chair" from – 60 °C to 60 °C. Substitution can also be explored to tailor an equilibrium position rationally, with diamide on opposing arenes that stabilizes "Boat" whereas ester favors "Chair". This low-energy driven DBCOD conformational interconversion, is expected to enable biological and materials applications, hitherto unattainable.

A low-energy driven molecular switch is a cornerstone phenomenon that empowers technologies like biomanipulators (e.g., tweezers and gear<sup>1</sup>, and ion channel regulation<sup>2</sup>), controlled drug release<sup>3</sup>, regenerative medicine (e.g., dynamic scaffolds<sup>4</sup>, and artificial muscle<sup>5</sup>), adaptive architectural systems (e.g., "heliophilic" optics<sup>6</sup>), soft robotics<sup>7,8</sup>, deployable structures (such as erectable trusses and inflatable solar concentrators)9-11, and memory and logic devices12,13. Conventional small organic molecular photoswitches are based on bond-forming cyclization or bond-breaking ring opening reactions as found in spiropyrans<sup>14,15</sup>, fulgides<sup>16-18</sup> and diarylethenes<sup>19,20</sup> systems, and configurational isomerization reactions, such as trans-cis interconversions of azobenzene<sup>21,22</sup> and stilbenes-containing<sup>23,24</sup> systems. These conventional switches intrinsically require high-energy ultraviolet (UV) light for upconversion, and consequentially responsible for photobleaching and biological incompatibility. Several decades of research have led to the development of photoswitches that respond to longer irradiation wavelengths like visible and infrared<sup>25-27</sup>. However, the new photoswitches lack recyclability. Intrinsically, photon stimuli are limited to approximately one micron of penetration depth due to competing absorption<sup>28</sup>. The latest photoswitches include the donor-acceptor Stenhouse adducts activated by visible light<sup>29-31</sup>. Limitations of this system include strong solvent dependence, spontaneous reversion without stimulation and lack of cycle stability. For biological and materials applications, new types of molecular switches that can be driven by low-energy stimuli (thermal) in ambient environments with robustness and reliability are highly sought after.

Nature provides an endless repertoire of conformational changes in response to chemical stimuli to drive and control diverse cellular processes. For instance, hemoglobin delivers oxygen through the body, and changes shape to bind carbon dioxide for disposal<sup>32</sup>. The conformational change of a G protein-coupled receptor (GPCR) activates a nearby G protein, leading to the production of secondary messengers. Through a sequence of events, GPCRs regulate an incredible range of bodily functions, from sensation to hormone responses<sup>33</sup>. Displaying efficiency, reliability and reproducibility, these molecular level conformational transitions serve as an inspirational model.

Dibenzocycloocta-1,5-diene, DBCOD, features a flexible eight-membered ring with rigid phenyl rings fused to each end (Fig. 1). We have described a number of examples whereby DBCOD-containing polymers exhibited significant thermal contraction<sup>34-36</sup> despite containing only a small amount of tetraphenylamide substituted DBCOD. Theoretical calculations implied that the origin of this substantial thermal contraction was the DBCOD conformational transition from the "Boat" conformation (global minimum) to the "Chair" conformation (local minimum) upon heating<sup>35</sup>.

To examine this hypothesis, we have synthesized a library of DBCODs bearing various substituents (Fig. 2). By combining variable temperature NMR (VT-NMR) spectroscopic characterizations with density functional theory (DFT) calculations, we discovered that "Boat" is the global minimum and we can significantly adjust DBCOD conformational dynamics by varying intramolecular interactions through substitution.

Trans- to cis- isomerization of azobenzene requires an activation energy at least 150

kJ/mol and very often in excess of 250 kJ/mol<sup>37,38</sup>. In stark contrast, the activation energy for conformational change of unsubstituted DBCOD is approximately 40 kJ/mol<sup>39</sup>. Our experimental and computational results indicate that DBCODs bearing aldehyde substituents on carbons 1 and 10 raise the activation energy ( $\Delta G^{\dagger}$ ) while 2, 9 substitution which is one atomic position away did not. That for 1, 10 dialdehyde substitution was 55 kJ/mol while 2, 9 dialdehyde substitution required 44 kJ/mol, as similar as an unsubstituted one.

Comparing ester with amide substitution,  $\Delta G^{\dagger}$  of ester, either diethylester or diphenylester was about 50 kJ/mol. The strong intramolecular hydrogen bonds imposed by 1,10-diamide substitution resulted in an activation energy of 68 kJ/mol, equivalent to near infrared light stimulus of 1500 to 1600 nm<sup>40</sup>. In living systems, enzymatic catalyzed conformational processes with similar activation energies<sup>41-43</sup>. In general, the activation energies for enzyme catalyzed biological reactions are approximately 54 – 84 kJ/mol, which is comparable to the activation energies of DBCOD conformational changes.

This is the first demonstration that conformational dynamics of a medium-sized hydrocarbon ring can be tailored by substitution. Substituent effects and mechanistic hypotheses described herein is expected to herald a new category of small molecule switches that are low-energy stimuli driven. This simple system is expected to enable technological exploration and facilitate the study of conformational change in our living systems.

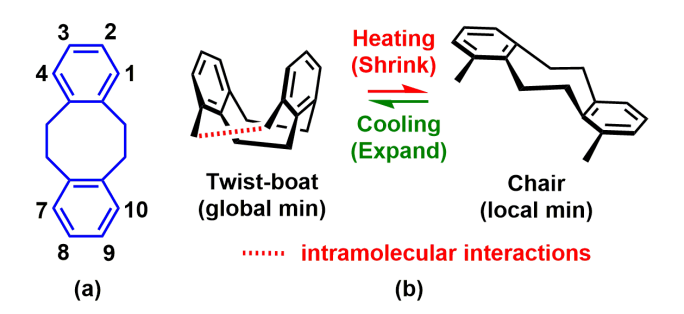


**Fig. 1** (a) Chemical structure of a DBCOD unit (in blue) and possible substitution positions (1-10). (b) Schematic drawing to illustrate intramolecular interaction to stabilize "Boat" and interconversion between "Boat" and "Chair".

#### Results and discussion

Here we designed a molecular hinge, DBCOD. An eight-membered ring, a flexible unit, is infused by two rigid benzene rings. To stabilize one of conformations formed by the flexible ring, we synthesized 2,3,8,9-tetramethyl DBCOD (TM-DBCOD) and its derivatives and investigated the effect of intra- and inter-molecular interactions on conformation preference and dynamics.

### Synthesis of Functional Group Substituted DBCOD Derivatives.

Fig. 2 Synthetic route of 2,3,8,9-tetramethyl DBCOD (TM-DBCOD) derivatives.

TM-DBCOD and 1,10 position di-substituted derivatives, including dialdehyde (1,10-di-CHO), diphenylester (1,10-di-Ph-ester), diethylester (1,10-di-Et-ester) and diphenylamide (1,10-di-Ph-amide) or diethylamide (1,10-di-Et-amide) substituted TM-DBCOD, were synthesized according to the synthetic route shown in Fig. 2.

The TM-DBCOD was synthesized from (4,5-dimethyl-1,2-phenylene)dimethanol (di-OH) with a large scale, sequentially through bromination<sup>44</sup> using phosphorous tribromide and dimerization<sup>45,46</sup> in the presence of lithium sands. 1,10-di-CHO was formed via Rieche formylation<sup>47,48</sup>. One-step column purification of 1,10-di-CHO was adequate without the need of multi-step column purification for the preparation of 2,9di-CHO<sup>49</sup>. Because there are only four possible positions for the formylation of TM-DBCOD, theoretically generating less by-products than that of 1,2:5,6dibenzocyclooctadiene (DBCOD). We found out that the 1,10 position-formylated isomer can be easily distinguished and separated from flash column purification<sup>47</sup>. Finally, 1,10-di-Et-ester, 1,10-di-Ph-ester, 1,10-di-Et-amide and 1,10-di-Ph-amide were successfully prepared stepwise through oxidation with hydrogen peroxide and sodium chlorite<sup>50</sup>, acyl chlorination using thionyl chloride and esterification/amidation based on different substrates, like alcohol or amine. The chemical structures of all these different functional group substituted DBCOD molecules were confirmed by <sup>1</sup>H and <sup>13</sup>C NMR. (Supplementary Fig. S1-S16)

#### Variable Temperature Nuclear Magnetic Resonance and DFT Calculations

Variable temperature nuclear magnetic resonance, VT-NMR, spectroscopy has been employed to study conformational changes of medium-sized rings<sup>51,52</sup>. VT-NMR

provides activation energy ( $\Delta G^{i}$ ) from the global minimum to transition state, as well as Gibbs free energy between "Boat" and "Chair" ( $\Delta G^{o}$ ). The coalescence temperature ( $T_{c}$ ) is defined as above which the rate of exchange between two conformational states is higher than the NMR experimental time scale. As a result, a single broadened resonance peak can be observed. Proton VT-NMR analysis of different DBCOD substituents were conducted using a deuterated solvent mixture, specifically polar  $CD_{2}Cl_{2}$  and non-polar  $CS_{2}$  with the volume ratio of 4/1 for TM-DBCOD, 1,10-di-CHO and diester substitutions, or polar solvent (DMSO-d<sub>6</sub>) for diamide substitutions. A mixture of DMSO-d<sub>6</sub> and  $CD_{2}Cl_{2}$  for 1,10-di-Ph-amide was further used to understand the effect of solvent polarity.

Density functional theory (DFT) calculation of <sup>1</sup>H NMR chemical shifts for the "Boat" and "Chair" isomers are summarized in Supplementary Table S1. These predicted chemical shift values helped to assign signals in <sup>1</sup>H NMR spectra (Fig. 3). Molecular symmetry difference caused by substitution along with different spatial arrangements for "Boat" and "Chair" afford multiple inequivalent methylene and methyl proton environments. Experimentally, ring dynamics simplifies the <sup>1</sup>H NMR spectra with increasing temperature by dynamically averaging the multiple chemical shifts. Further, DFT calculations predict optimal molecular structures and relative energies of all DBCOD derivatives in "Boat", transition state and "Chair" conformations.

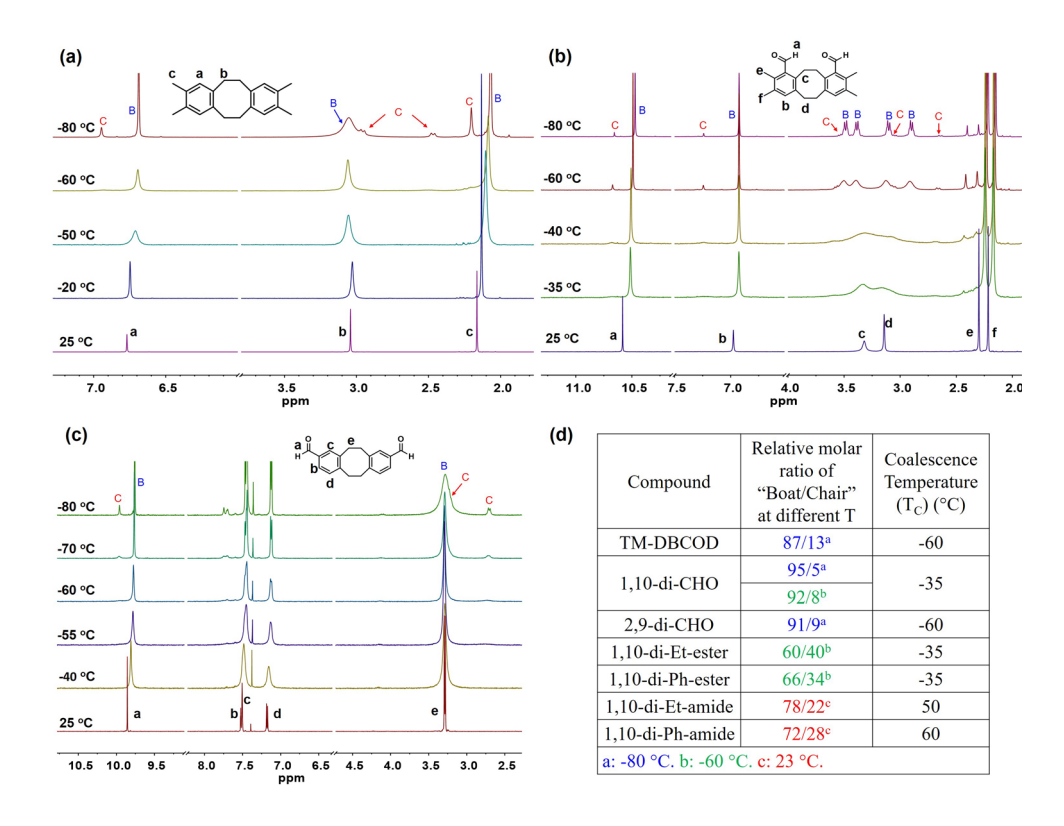


Fig. 3 VT- $^{1}$ H NMR of (a) TM-DBCOD, (b) 1,10-di-CHO and (c) 2,9-di-CHO. (d) Relative molar ratio of "Boat/Chair" for different DBCOD derivatives at different temperatures and the corresponding  $T_{\rm c}$ .

Taking TM-DBCOD at -80 °C as an example (Fig. 3a), the aromatic protons gave two signals ( $\delta = 6.95$  and 6.69 ppm) and the methylene protons gave one broad signal along with two doublets,  $\delta = 3.05$ , 2.96 (J = 11.8 Hz) and 2.47 (J = 11.9 Hz) ppm. Previous reports<sup>53,54</sup> stated that two nonequivalent protons on "Chair" should generate an AB quartet (four lines), whereas the "Boat" conformation should exhibit two AB quartet patterns (eight lines). If the temperature was sufficiently low to slow down the inversion of "Boat" conformers, two quartet peaks should show up. Even at -80 °C the multiple methylene resonances predicted for the "Boat" configuration were not resolved demonstrating that there were ring dynamics present at this low temperature.

The high-intensity and broad peak centered at 3.05 ppm was ascribed to "Boat" whereas two doublets were ascribed to "Chair". Our simulated NMR spectrum (Supplementary Table S1) also confirmed that the upfield-shifted (low frequency) methylene signals (- $CH_2$ -) between 2.9 and 2.6 ppm belonged to "Chair", whereas "Boat" - $CH_2$ - are predicted to occur between 3.43 and 2.77 ppm.

Using the integrals of two sets of either aromatic or tetramethyl protons, the population of "Chair" was determined to be 13% whereas the population of "Boat" was 87% respectively. At -60 °C, NMR chemical shifts, including aromatic proton ( $\delta$  = 6.77 ppm) and methylene proton on eight-membered ring ( $\delta$  = 3.04 ppm), appeared as broadened singlets due to fast exchange. It was known that the population of "Chair" and "Boat" dictated NMR chemical shift. The fact that the NMR resonance belonging to aromatic proton moved towards "Chair" was indicative of "Chair" population increasing with temperature.

For 1,10-di-CHO at low temperatures (-80 and -60 °C) (Fig. 3b), the de-shielded aldehyde and aromatic protons split into two singlets at  $\delta = 10.66$  and 10.47 ppm, and at  $\delta = 7.24$  and 6.92 ppm respectively. The tetramethyl protons gave two sets of two singlets ( $\delta = 2.40$ , 2.30 ppm and  $\delta = 2.21$ , 2.15 ppm), while the methylene protons appeared a series of multiplets. The more intense set ( $\delta = 3.49$ , 3.39, 3.10, 2.90 ppm) corresponded to the different chemical environments of -C $H_2$ - on the eight-member ring in the "Boat" conformer (Supplementary Table S1). Another minor set of resonances observed at -80 °C was the tiny singlet from aldehyde proton at 10.66 and aromatic proton at 7.24 ppm, together with the doublets from methylene protons at 3.54,

2.64 ppm, indicating the presence of a small portion of "Chair" conformer. The relative populations of "Boat" and "Chair" can be calculated using either aldehyde or aromatic or tetramethyl proton as 95 % "Boat", and 5 % "Chair", respectively at – 80 °C. Comparing with TM-DBCOD at the same temperature of 87% "Boat" and 13% "Chair", we thus concluded that substitution stabilizes "Boat". The coalescence temperature (T<sub>c</sub>) was observed to increase from – 60 °C of TM-DBCOD to – 35 °C of 1,10-di-CHO.

Moreover, we compared the VT-NMR spectra of 2,9-di-CHO (Fig. 3c) that is one atomic position away from the eight-membered ring in contrast to 1,10-di-CHO. The calculated relative populations of "Boat" and "Chair" for 2,9-di-CHO at – 80 °C were 91 % and 9 %, using integrals of either the aldehyde proton signal at 9.76 ppm for "Boat" and 9.96 ppm for "Chair or the methylene proton signal at 3.28 ppm for "Boat" and 3.20, 2.70 ppm for "Chair", respectively. The observed T<sub>c</sub> of 2,9-di-CHO was similar to that for unsubstituted TM-DBCOD. This result indicated the importance of substitution position on the DBCOD kinetics and energetics. Moving the substitution position next to the central eight-membered ring, T<sub>c</sub> elevated from – 60 °C of 2,9-di-CHO to – 35 °C of 1,10-di-CHO.

According to NMR chemical shift prediction, in the  $^{1}$ H NMR spectrum of 1,10-di-Et-ester at  $-60^{\circ}$ C (Fig. 4a), four sets of methylene doublets at 2.38, 2.55, 2.77 and 3.02 ppm were assigned to the "Chair" conformation. Two broad peaks at 2.98 and 3.10 ppm belonged to "Boat". The integrals of two sets of tetramethyl protons yielded relative population percentage that is 40% "Chair" and 60% "Boat". This was in contrast to the 1,10-di-CHO at  $-60^{\circ}$ C with 8 % "Chair" and 92 % "Boat".

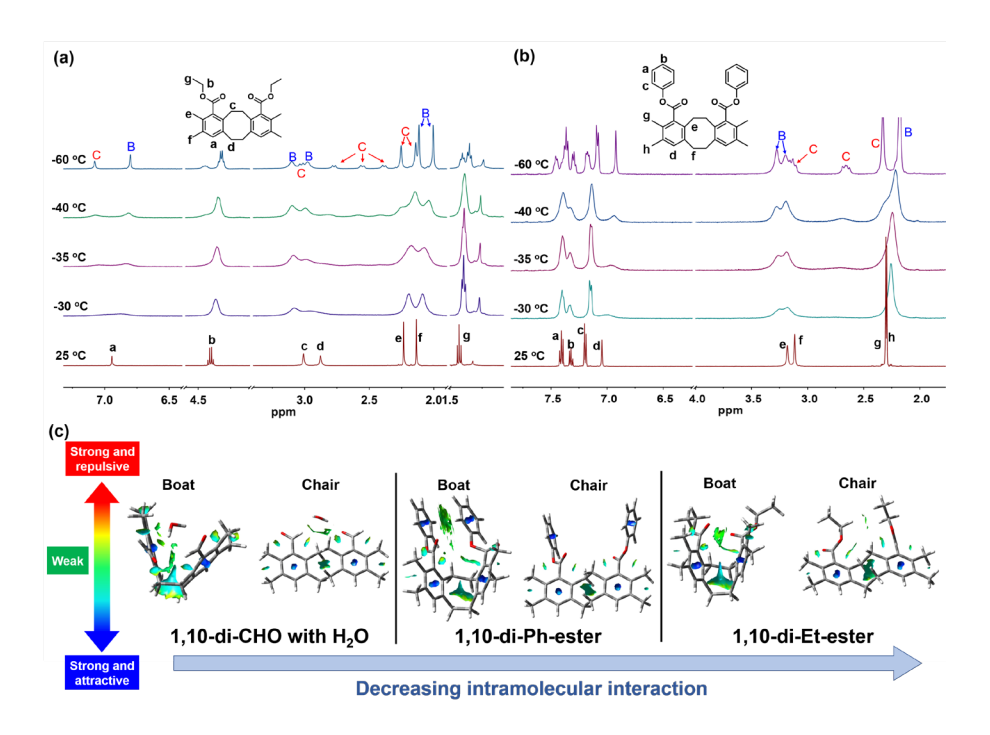


**Fig. 4** VT-<sup>1</sup>H NMR of (a) 1,10-di-Et-ester and (b) 1,10-di-Ph-ester. (c) NCI plots based on DFT calculation of DBCOD derivatives in the "Boat" and "Chair" conformations for 1,10-di-CHO with one water molecule encased (left), 1,10-di-Ph-ester (middle) and 1,10-di-Et-ester (right). (black: carbon; white: hydrogen; red: oxygen).

There was a small presence of water ( $\delta$  = 1.54 ppm in <sup>1</sup>H NMR spectrum of 1,10-di-CHO) encased in between two aldehyde groups to form intramolecular hydrogen bonds. This contention was confirmed by differential scanning calorimetry analysis (Supplementary Fig. S17). Non-covalent interaction (NCI) plots (Fig. 4c) revealed the effect of intramolecular interaction. In comparison with 1,10-di-Et-ester,  $\pi$ - $\pi$  interaction of two extended benzene rings in 1,10-di-Ph-ester can stabilize "Boat". At – 60 °C, 1,10-di-Ph-ester yielded higher "Boat" population of 66 % as opposed to 60 % "Boat" of 1,10-di-Et-ester (Fig. 3d). As a result of strong intra-hydrogen bonds formed with an encased water molecule and aldehyde groups, 92 % "Boat" was available in

1,10-di-CHO at -60 °C. Electrostatic repulsive interaction between two adjacent ethyl ester groups of 1,10-di-Et-ester can actually stabilize "Chair" further, 5 times higher "Chair" population, 40 % "Chair" for 1,10-di-Et-ester vs 8 % "Chair" in 1,10-di-CHO at -60 °C (Fig. 3d). Replacing phenyl ring of ethyl group in diester DBCODs can mitigate this repulsive interaction in couple with  $\pi$ - $\pi$  interaction shifted the equilibrium to the "Boat" conformer. Therefore, at -60 °C, 1,10-di-Ph-Ester offered 34% "Chair", less than that of 1,10-di-Et-ester. The electron density maps (Supplementary Fig. S18) of diester substituted DBCODs agreed well with the VT-NMR results (Fig. 3d).

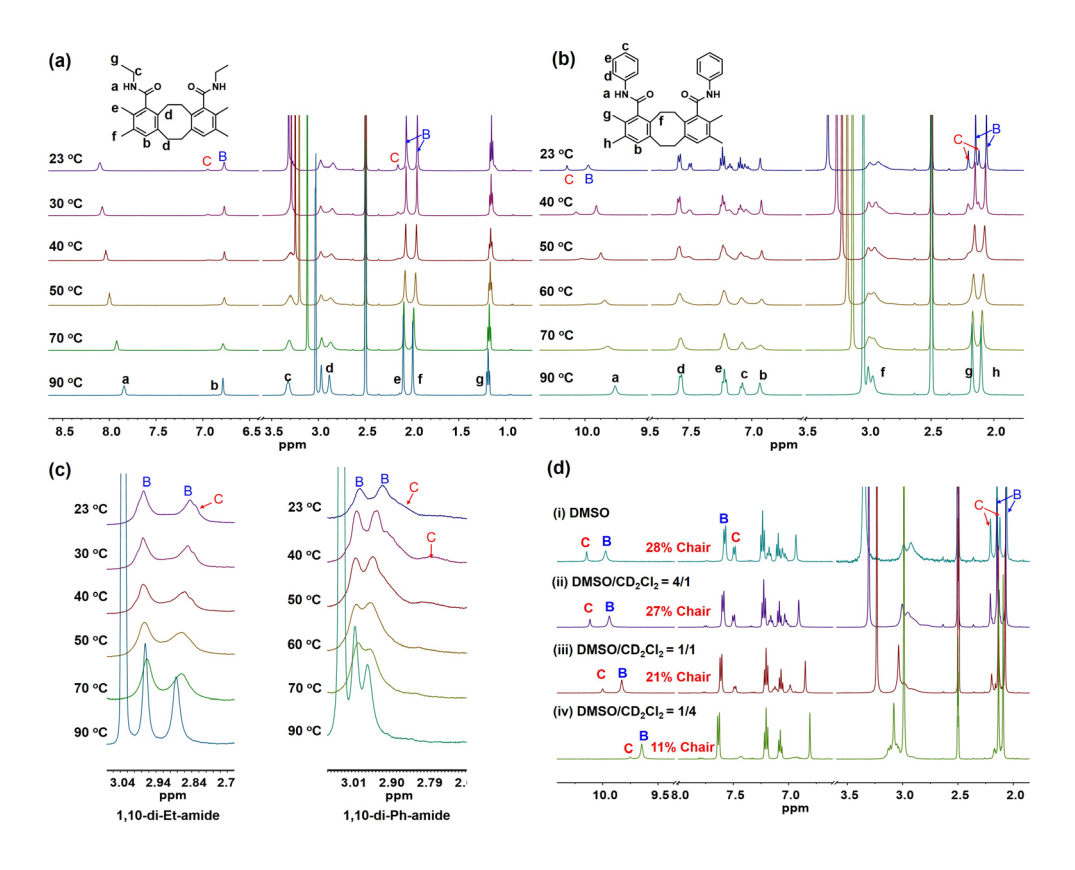


**Fig. 5** VT-<sup>1</sup>H NMR spectra of (a) 1,10-di-Et-amide, (b) 1,10-di-Ph-amide and (c) the methylene protons for both. (d) <sup>1</sup>H NMR spectra of 1,10-di-Ph-amide in different deuterated solvents.

The DFT NMR predictions (Supplementary Table S1) indicated tetramethyl protons in "Chair" configuration should move to downfield. VT  $^1$ H-NMR of 1,10-di-Et-amide (Fig. 5a) at low temperature displayed two sets of peaks for both aromatic and tetramethyl protons. According to theory calculation, the methyl proton at  $\delta = 2.15$  ppm was ascribed to "Chair", while  $\delta = 2.06$  and 1.94 ppm resonances were assigned to "Boat". One could rationally deduce that two aromatic proton peaks corresponded to "Chair" ( $\delta = 6.95$  ppm) and "Boat" ( $\delta = 6.77$  ppm) respectively with relative populations of 22% "Chair" and 78% "Boat" at 23 °C.  $T_c$  was detected at about 50 °C. The results were consistent with the postulation that intramolecular hydrogen bonding can raise the activation energy for the dynamic conversion of the different isomers.

Similar to 1,10-di-Et-amide, the VT  $^1$ H NMR spectra of 1,10-di-Ph-amide (Fig. 5b) also displayed both two sets of peaks associated with aromatic and tetramethyl protons. Based on calculated chemical shifts, we assigned tetramethyl protons at  $\delta = 2.20$ , 2.12 ppm to "Chair" conformation whereas the  $\delta = 2.15$ , 2.06 ppm to "Boat". Peak integration of either aromatic or tetramethyl protons indicated that the relative population of "Chair" and "Boat" was about 28% and 72% respectively at 23 °C. The "Chair" population was 6 % higher than that of 1,10-di-Et-amide at the same temperature, most likely due to the steric hindrance effect generated by phenyl rings. The  $T_c$  was observed at 60 °C. Proton chemical shift of methylene of the eightmembered ring (Fig. 5c) also confirmed that the conformational transitions for diamide derivatives in DMSO occurs at room temperature or above. The averaged two singlets

of methylene proton at 90 °C ( $\delta$  = 2.96, 3.0 ppm for 1,10-di-Ph-amide, and  $\delta$  = 2.97, 2.88 ppm for 1,10-di-Et-amide) were transformed into two broadened resonances with shoulder peaks at 40 °C and below, indicating the slow exchange of "Boat" and "Chair".

It is known that solvent can affect barrier height of isomerization<sup>55-57</sup>. To examine the effect of solvent property on the DBCOD conformational dynamics, we performed <sup>1</sup>H NMR using different volume ratios of deuterated DMSO to DCM which is a less polar solvent (Fig. 5d). "Boat" population increased with reducing the amount of DMSO in the solvent mixture, suggesting that DSMO can break the DBCOD intramolecular hydrogen bond and destabilize "Boat".

# Comparison of Experimental Data with Theory Calculations on DBCOD conformational dynamics

We also calculated the DBCOD conformational exchange rate. Supplementary Table S2 displayed exchange rates between "Boat" and "Chair", entropy of activation ( $\Delta S^{\dagger}$ ), and enthalpy of activation ( $\Delta H^{\dagger}$ ) of various DBCOD derivatives. Negative entropy of activation was observed. Calculated values for  $\Delta H^{\dagger}$  were similar for all molecules but  $\Delta S^{\dagger}$  values varied significantly. The greater the intramolecular force formed by two substitution groups exists, the more negative  $\Delta S^{\dagger}$  value will be. The negative  $\Delta S^{\dagger}$  implied the intramolecular interaction reduced the number of degrees of freedom for molecular motion and led to a higher entropic penalty for activation of conformational change. This result confirmed that substitution can be used to tailor the reaction kinetics through entropy of activation (Fig. 6a). Studies in azobenzene isomerization also revealed the

negative entropy<sup>55,57-59</sup>, indicating the activated complex during isomerization was more ordered.

Compared to unsubstituted TM-DBCOD with an activation energy of 42.0 kJ/mol, 2,9-di-CHO did not have a significant effect on interconversion with an activation energy of 44.4 kJ/mol (Supplementary Table S3). Weak interaction between adjacent phenyl ester and ethyl ester groups yielded an activation energy of about 50 kJ/mol. Strong intramolecular hydrogen bonding formed between the adjacent amide groups (HNC=O···HNC=O) gave rise to an activation energy of ~ 70 kJ/mol, over 60 % higher than the value obtained from the unsubstituted TM-DBCOD. This result indicates that hydrogen bonding stabilized "Boat" by elevating activation energy. Similarly, the weak hydrogen bonds between water and the pair of CHO groups led to activation energy of 55.1 kJ/mol. There is an excellent agreement between DFT calculations and experimental results (Fig. 6a).

Furthermore,  $\Delta H^{\dagger}$  varies linearly with  $\Delta S^{\dagger}$  as a function of  $\Delta H^{\dagger}$ =45.68+0.11 $\Delta S^{\dagger}$  (Supplementary Fig. S19). Thus, the DBCOD conformational change exhibited a typical enthalpy-entropy compensation effect<sup>60</sup>. This demonstrated that substitution did not alter either the reaction pathway or mechanism. Analogously, enthalpies of activation for the *cis-trans* isomerization among azobenzene-based molecules with different substitutions were similar and not sensitive to substitution properties<sup>58</sup>.

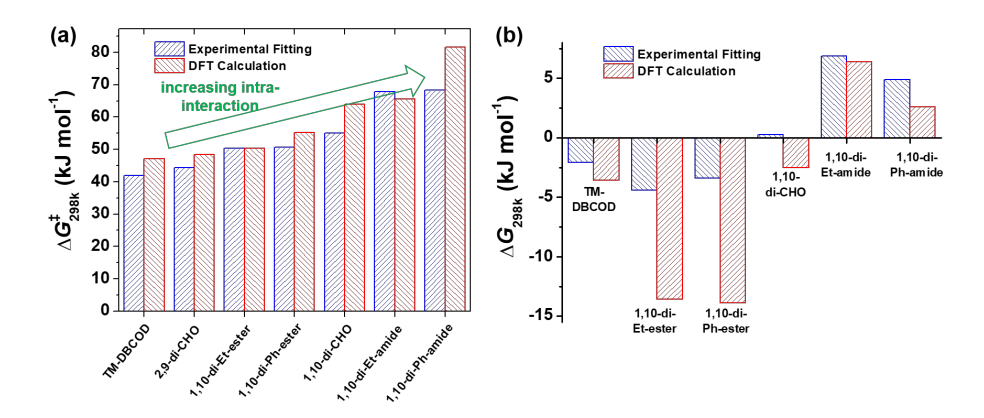


**Fig. 6** (a) Kinetic and (b) energetic Gibbs free energy changes of DBCOD derivatives at 298 K.

DFT predicted that intramolecular forces can significantly influence the energetic of DBCODs' conformational change from "Boat" to "Chair". Intramolecular interaction generated by hydrogen bonding and  $\pi$ - $\pi$  interaction steered the equilibrium position towards "Boat". This trend foreseen by computation was in accordance with experimental data (Fig. 6b and Table S3). Without intramolecular interaction, "Chair" conformers of TM-DBCOD possessed lower energy level at 298 K, favoring "Chair". Due to low activation energy, "Boat" and "Chair" can exchange autonomously. Because of the electrostatic repulsive interaction, 1,10-di-Ph-ester and 1,10-di-Et-ester demonstrated much more negative  $\Delta G^{o}$  than that of TM-DBCOD, which agreed well with the electron density map (Fig. S18). The difference between experimental-fitted and DFT calculated  $\Delta G^{\circ}$  of 1,10-di-CHO is due to the inserted water molecule beside two adjacent CHO groups not considered in DFT prediction. By including water molecule in between two CHO groups, the formed hydrogen bonding could stabilize "Boat" conformer and prompt "Boat" as the global minimum. For 1,10-di-Et-amide and 1,10-di-Ph-amide, an intramolecular hydrogen bond formed by adjacent diamide groups rendered "Boat" as the global minimum. Preference of "Boat" over "Chair" resulted in a positive value of  $\Delta G^{\circ}$  at 298 K. The more positive the value is, the higher population of "Boat". Indeed, at 23 °C, we observed 78 % "Boat" in 1,10-di-Et-amide and 72 % "Boat" in 1,10-di-Ph-amide. In stark contrast, unsubstituted DBCOD could sustain 87% "Boat" only at -80 °C. 100 °C difference indicates the intramolecular hydrogen bonding significantly increased the upconversion barrier from "Boat" to "Chair".

#### **Small-molecule X-ray Crystallography**

DFT calculations in solid state indicates that "Chair" became more favorable for non-intramolecular attracted DBCOD derivatives, due to intermolecular  $\pi$ - $\pi$  interaction between phenyl rings on DBCOD. For example, two TM-DBCOD molecules will favor "Chair" by reducing the  $\Delta G^o$  value by 5.9 kJ/mol, compared with single molecule. Based on X-ray crystallographic characterization, the molecular structures and crystal packings for TM-DBCOD and 1,10-di-Et-amide, have been identified (Fig. 7). Without substitution, TM-DBCODs were all in the "Chair" conformation, in a good agreement with the published result of DBCOD without tetramethyl substitutions<sup>61</sup>.

However, 1,10-di-Et-amide existed in the "Boat" conformation in solid. The intramolecular hydrogen bonding was sufficiently strong to compel molecules to packed as "Boat", simultaneously encouraged  $\pi$ - $\pi$  interaction along two sides of each "Boat". This finding also reinforced our conclusion that substitution played a profound role on conformational preference.

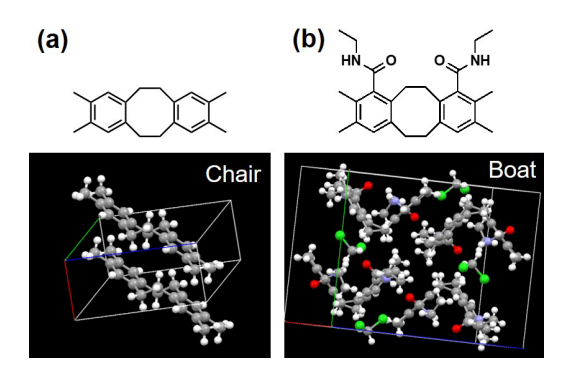


**Fig. 7** Molecular structure and crystal packing of (a) TM-DBCOD and (b) 1,10-di-Et-amide. red: Oxygen, purple: Nitrogen, green: Chlorine (solvent) and dark gray: Carbon.

#### Conclusion

Substitution has been proven as a powerful tool that potentially transform DBCOD conformational change into a low-energy switching event. TM-DBCOD required just 42 kJ/mol for upconversion from "Boat" to "Chair." Substitution can raise the upconversion barrier up to 68 kJ/mol by stabilizing "Boat" over "Chair". The activation energy requires for this conformational change lay within the enzyme catalyzed biological reactions and make this switch one of its kind. This work is expected to lay the foundation for scientific exploration of this new switching mechanism. A low-energy driven reversible conformational change that can be triggered by a broad range of stimuli such as heating, IR induced or magnetic induction at either a few degrees above room or physiological relevant temperature, can potentially enable many applications. For example, it can be tethered onto biomolecules and incorporated in a polymer to achieve desired functionality. Large geometrical change in response to ambient temperature fluctuations can be harnessed for heliotropism. The geometrical change can also be exploited to enable pore size modulation of polymer membranes for

applications in energy and health. DBCOD embedded polymeric electronic packaging materials could reduce polymer thermal expansion and thus improve reliability of high-density memory devices and possibly realize higher speed logical devices, just to name a few.

#### Methods

Materials. (4,5-dimethyl-1,2-phenylene)dimethanol (di-OH) (>95 %, Ryan Scientific Inc.), phosphorus tribromide (PBr<sub>3</sub>, 99%, ACROS Organics), sodium bicarbonate (NaHCO<sub>3</sub>, >99.7 %, Fisher Scientific), methylene chloride (DCM, Stabilized/Certified ACS, Fisher Chemical), Lithium granules (Li, 1-6 mm (0.04-0.2 in.), 99% (Metals basis), Alfa Aesar), Tin(IV) Chloride (SnCl<sub>4</sub>, anhydrous 99%, ACROS Organics), dichloromethyl methyl ether (>97 %, TCI America), sodium phosphate monobasic monohydrate (NaH<sub>2</sub>PO<sub>4</sub>·H<sub>2</sub>O, Crystalline/Certified ACS, Fisher Chemical), hydrogen peroxide (H<sub>2</sub>O<sub>2</sub>, 30 wt%, Certified ACS, Fisher Chemical), sodium chlorite (NaClO<sub>2</sub>, 80% pure, unstabilized, ACROS Organics), thionyl chloride (SOCl<sub>2</sub>, ≥99%, Sigma-Aldrich), phenol (Liquid/Certified ACS, Fisher Chemical), ethylamine (2 M in THF solution, Sigma-Aldrich), aniline (ACS reagent, ≥99.5%, Sigma-Aldrich) were used as received without further purification. All other chemical reagents were purchased from either Sigma-Aldrich or Fisher and used without further purification.

**Characterizations.** <sup>1</sup>H and <sup>13</sup>C NMR spectra were recorded on a 500 MHz Agilent system and the variable temperature <sup>1</sup>H NMR (VT-NMR) spectra were recorded on a Bruker Avance500 II spectrometer. The residual solvent proton signal was used as the

reference peak. Matrix-assisted laser desorption ionization (MALDI) mass spectra were measured on 4800 MALDI TOF/TOF analyzer from Applied Biosystems. Thermal transition behaviors and heat capacities were measured using a TA Q2000 DSC instrument with the nitrogen flow rate of 100 mL/min. Single crystals of TM-DBCOD and 1,10-di-Et-amide were prepared by vapor diffusion technique in a closed system from the 1 mg/mL sample's DCM solution in an inner open vial with methanol in the outer vial. X-ray crystallography investigation was carried out at 100 K using a Bruker APEX II CCD diffractometer on Beamline 11.3.1 at the Advanced Light Source at the Lawrence Berkeley National Laboratory.

**DFT calculations.** The <sup>1</sup>H chemical shielding tensors ( $\sigma$ ) for the DBCOD derivatives were obtained using Gaussian 09 with the gauge-including atomic orbital (GIAO) method at the DFT level<sup>62</sup>. The structures were optimized using density functional theory (DFT) using an the B3LYP 6-311++G(d,p) basis set and exchange functional. The optimized structures were obtained in the gas phase. The NMR chemical shieldings were also calculated using the B3LYP 6-311++G(d,p) basis set for the different solvation models. The NMR chemical shift ( $\delta$ ) for each proton in the DBCOD species were calculated from the isotropic component of the tensor  $\sigma_{iso}$  a known reference shielding tensor using  $\delta = 31.97 - \sigma_{iso}$ .

NMR fitting for the evaluation of energy barrier to conformational exchange.

DBCOD derivatives were subjected to <sup>1</sup>H NMR measurements at various temperatures.

For each compound a region of the NMR spectrum that showed exchange characteristics was selected and the signals from that region were used for bandshape

analysis. Bandshape analysis was performed using the DNMR plugin in the Topspin software package (Bruker Biospin Corporation, Version 3.6.1, Billerica, 2018). Detailed information about rate constants, entropy of activation ( $\Delta S^{\dagger}$ ) and enthalpy of activation ( $\Delta H^{\dagger}$ ) for conformational change can be found in Supplementary material.

#### Acknowledgments

We really appreciate the financial support from NSF CHE-1900647 and National Aeronautics and Space Administration (NASA) grant no. NNX15AQ01. The NMR shielding calculation were performed at Sandia National Laboratories is a multimission laboratory managed and operated by National Technology and Engineering Solutions of Sandia, LLC., a wholly owned subsidiary of Honeywell International, Inc., for the U.S. Department of Energy's National Nuclear Security Administration under contract DE-NA0003525. The Work at the Molecular Foundry was supported by the Office of Science, Office of Basic Energy Sciences, of the U.S. Department of Energy under Contract No. DE-AC02-05CH11231.

#### Author contributions.

J.Q.L. and W.F. conceived the project and wrote the manuscript. W.F., J.B. and T.L. performed the synthesis and characterizations of all DBCOD derivatives. W.F. and Y.L. conducted the VT-NMR measurements. J.L., W.T. and T.M.A. performed the DFT calculations to reveal kinetics and energies at different states. T.M.A. performed the predicted <sup>1</sup>H NMR chemical shifts of DBCOD derivatives. R.W.A. evaluated the energy barrier for conformational exchange of DBCOD derivatives based on the VT-

NMR results. S.T. conducted the X-ray single-crystal diffraction measurements. W.F.,

R.W.A., S.T., B.J.S., T.M.A., W.Y., Y.L., and J.Q.L discussed about the data processing and revised the manuscript.

#### **Competing interests**

The authors declare no competing interests.

#### **References:**

- 1. Kamiya, Y. & Asanuma, H. Light-Driven DNA Nanomachine with a Photoresponsive Molecular Engine. *Accounts Chem. Res.* **47**, 1663-1672, (2014).
- 2. Li, X. et al. Role of outer surface probes for regulating ion gating of nanochannels. Nat. Commun. 9, 40, (2018).
- 3. Mura, S., Nicolas, J. & Couvreur, P. Stimuli-responsive nanocarriers for drug delivery. *Nat. Mater.* **12**, 991-1003, (2013).
- 4. Zeng, Y. & Lu, J. Q. Optothermally Responsive Nanocomposite Generating Mechanical Forces for Cells Enabled by Few-Walled Carbon Nanotubes. *ACS Nano* **8**, 11695-11706, (2014).
- 5. Lancia, F., Ryabchun, A., Nguindjel, A.-D., Kwangmettatam, S. & Katsonis, N. Mechanical adaptability of artificial muscles from nanoscale molecular action. *Nat. Commun.* **10**, 4819, (2019).
- Li, C. S., Liu, Y., Huang, X. Z. & Jiang, H. R. Direct Sun-Driven Artificial Heliotropism for Solar Energy Harvesting Based on a Photo-Thermomechanical Liquid-Crystal Elastomer Nanocomposite. *Adv. Funct. Mater.* 22, 5166-5174, (2012).
- 7. Aßhoff, S. J. *et al.* High-Power Actuation from Molecular Photoswitches in Enantiomerically Paired Soft Springs. *Angew. Chem. Int. Edit.* **56**, 3261-3265, (2017).
- 8. White, T. J. & Broer, D. J. Programmable and adaptive mechanics with liquid crystal polymer networks and elastomers. *Nat. Mater.* **14**, 1087-1098, (2015).
- 9. Cadogan, D. & Scarborough, S. in 19th AIAA Applied Aerodynamics Conference.
- Rossiter, J., Takashima, K., Scarpa, F., Walters, P. & Mukai, T. Shape Memory Polymer Hexachiral Auxetic Structures with Tunable Stiffness. Smart Mater. Struct. 23, 045007, (2014).
- 11. Takashima, K. *et al.* Pneumatic Artificial Rubber Muscle Using Shape-Memory Polymer Sheet With Embedded Electrical Heating Wire. *Smart Mater. Struct.* **23**, (2014).
- 12. Hou, L. *et al.* Optically switchable organic light-emitting transistors. *Nat. Nanotechnol.* **14**, 347-353, (2019).
- 13. Leydecker, T. *et al.* Flexible non-volatile optical memory thin-film transistor device with over 256 distinct levels based on an organic bicomponent blend. *Nat. Nanotechnol.* **11**, 769-775, (2016).
- 14. Klajn, R. Spiropyran-based Dynamic Materials. Chem. Soc. Rev. 43, 148-184, (2014).
- 15. Kohl-Landgraf, J. et al. Ultrafast Dynamics of a Spiropyran in Water. J. Am. Chem. Soc. 134,

- 14070-14077, (2012).
- 16. De Wergifosse, M., Houk, A. L., Krylov, A. I. & Elles, C. G. Two-photon absorption spectroscopy of trans-stilbene, cis-stilbene, and phenanthrene: Theory and experiment. *J. Chem. Phys.* **146**, (2017).
- de Villeneuve, C. H., Michalik, F., Chazalviel, J. N., Rück-Braun, K. & Allongue, P. Quantitative IR Readout of Fulgimide Monolayer Switching on Si(111) Surfaces. *Adv. Mater.* **25**, 416-421, (2013).
- 18. Yokoyama, Y. Fulgides for Memories and Switches. Chem. Rev. 100, 1717-1740, (2000).
- Fukaminato, T., Ishida, S. & Métivier, R. Photochromic fluorophores at the molecular and nanoparticle levels: fundamentals and applications of diarylethenes. NPG Asia Materials 10, 859-881, (2018).
- Guo, X., Zhou, J., Siegler, M. A., Bragg, A. E. & Katz, H. E. Visible-Light-Triggered Molecular Photoswitch Based on Reversible E/Z Isomerization of a 1,2-Dicyanoethene Derivative. *Angew. Chem. Int. Edit.* 54, 4782-4786, (2015).
- 21. Samanta, D. *et al.* Reversible photoswitching of encapsulated azobenzenes in water. *Proceedings of the National Academy of Sciences* **115**, 9379-9384, (2018).
- 22. Bandara, H. M. D. & Burdette, S. C. Photoisomerization in different classes of azobenzene. *Chem. Soc. Rev.* **41**, 1809-1825, (2012).
- 23. Quick, M. *et al.* Photoisomerization Dynamics of Stiff-Stilbene in Solution. *J. Phys. Chem. B* **118**, 1389-1402, (2014).
- 24. Feringa, B. L., van Delden, R. A., Koumura, N. & Geertsema, E. M. Chiroptical molecular switches. *Chem. Rev.* **100**, 1789-1816, (2000).
- 25. Pianowski, Z. L. Recent Implementations of Molecular Photoswitches into Smart Materials and Biological Systems. *Chemistry A European Journal* **25**, 5128-5144, (2019).
- 26. Dong, M. *et al.* Near-Infrared Photoswitching of Azobenzenes under Physiological Conditions. *J. Am. Chem. Soc.* **139**, 13483-13486, (2017).
- 27. Hammerich, M. *et al.* Heterodiazocines: Synthesis and Photochromic Properties, Trans to Cis Switching within the Bio-optical Window. *J. Am. Chem. Soc.* **138**, 13111-13114, (2016).
- 28. Yoshino, T. *et al.* Three-Dimensional Photomobility of Crosslinked Azobenzene Liquid-Crystalline Polymer Fibers. *Adv. Mater.* **22**, 1361-1363, (2010).
- 29. Zulfikri, H. *et al.* Taming the Complexity of Donor-Acceptor Stenhouse Adducts: Infrared Motion Pictures of the Complete Switching Pathway. *J. Am. Chem. Soc.* **141**, 7376-7384, (2019).
- 30. Lerch, M. M., Szymanski, W. & Feringa, B. The (photo)chemistry of Stenhouse photoswitches: guiding principles and system design. *Chem. Soc. Rev.* 47, 1910-1937, (2018).
- 31. Hemmer, J. R. *et al.* Controlling Dark Equilibria and Enhancing Donor-Acceptor Stenhouse Adduct Photoswitching Properties through Carbon Acid Design. *J. Am. Chem. Soc.* **140**, 10425-10429, (2018).
- 32. Perutz, M. F. Mechanisms Regulating the Reactions of Human Hemoglobin With Oxygen and Carbon Monoxide. *Annu. Rev. Physiol.* **52**, 1-26, (1990).
- 33. Li, J. et al. The Molecule Pages database. Nature 420, 716-717, (2002).
- 34. Ugur, G., Chang, J., Xiang, S., Lin, L. & Lu, J. A near-infrared mechano responsive polymer system. *Adv. Mater.* **24**, 2685-2690, (2012).
- 35. Shen, X., Viney, C., Johnson, E. R., Wang, C. & Lu, J. Q. Large Negative Thermal Expansion of A Polymer Driven by A Submolecular Conformational Change. *Nat. Chem.* **5**, 1035-1041,

- (2013).
- 36. Shen, X. *et al.* Adjusting Local Molecular Environment for Giant Ambient Thermal Contraction. *Macromol. Rapid Commun.* **37**, 1904-1911, (2016).
- 37. Weston, C. E., Richardson, R. D., Haycock, P. R., White, A. J. P. & Fuchter, M. J. Arylazopyrazoles: Azoheteroarene Photoswitches Offering Quantitative Isomerization and Long Thermal Half-Lives. *J. Am. Chem. Soc.* **136**, 11878-11881, (2014).
- 38. Crecca, C. R. & Roitberg, A. E. Theoretical Study of the Isomerization Mechanism of Azobenzene and Disubstituted Azobenzene Derivatives. *J. Phys. Chem. A* **110**, 8188-8203, (2006).
- 39. Crossley, R. *et al.* Conformational Behavior of Medium-Sized Rings. Part 1. 5,6,11,12-Tetrahydrodibenzo[a,e]cyclo-octene (1,2,5,6-Dibenzocyclo-Octa-1,5-Diene) and Heterocyclic Analogs. *J. Chem. Soc.-Perkin Trans.* 1, 205-217, (1973).
- 40. Allisy-Roberts, P. & Williams, J. in *Farr's Physics for Medical Imaging (Second Edition)* (eds Penelope Allisy-Roberts & Jerry Williams) 1-21 (W.B. Saunders, 2008).
- 41. Hu, H., Boone, A. & Yang, W. Mechanism of OMP Decarboxylation in Orotidine 5'-Monophosphate Decarboxylase. *J. Am. Chem. Soc.* **130**, 14493-14503, (2008).
- Kuhn, B. & Kollman, P. A. QM-FE and Molecular Dynamics Calculations on Catechol O-Methyltransferase: Free Energy of Activation in the Enzyme and in Aqueous Solution and Regioselectivity of the Enzyme-Catalyzed Reaction. J. Am. Chem. Soc. 122, 2586-2596, (2000).
- 43. Massey, V., Curti, B. & Ganther, H. A Temperature-Dependent Conformational Change in D-Amino Acid Oxidase and Its Effect on Catalysis. *J. Biol. Chem.* **241**, 2347-&, (1966).
- 44. Levick, M. T. *et al.* Phase Tag-Assisted Synthesis of Benzo[b]carbazole End-Capped Oligothiophenes. *Org. Lett.* **14**, 5744-5747, (2012).
- 45. Baker, W., Banks, R., Lyon, D. R. & Mann, F. G. 10. The Action of Sodium on o-Xylylene Dibromide. *J. Chem. Soc.*, 27-30, (1945).
- 46. Hamza, A. Gas-phase conformations and exciton couplings in 5,6,11,12-tetrahydrodibenzo[a,e]cyclooctene. *Struct. Chem.* **21**, 787-793, (2010).
- 47. Sekine, Y. & Boekelheide, V. A study of the synthesis and properties of [26](1,2,3,4,5,6)cyclophane (superphane). J. Am. Chem. Soc. 103, 1777-1785, (1981).
- 48. Sekine, Y., Brown, M. & Boekelheide, V. [2.2.2.2.2.2](1,2,3,4,5,6)Cyclophane: superphane. *J. Am. Chem. Soc.* **101**, 3126-3127, (1979).
- 49. Wang, Z. *et al.* Design and Synthesis of Thermal Contracting Polymer with Unique Eight-Membered Carbocycle Unit. *Macromolecules* **51**, 1377-1385, (2018).
- 50. Dalcanale, E. & Montanari, F. Selective Oxidation of Aldehydes to Carboxylic Acids with Sodium Chlorite-Hydrogen Peroxide. *J. Org. Chem.* **51**, 567-569, (1986).
- 51. Witosińska, A., Musielak, B., Serda, P., Owińska, M. & Rys, B. Conformation of Eight-Membered Benzoannulated Lactams by Combined NMR and DFT Studies. *J. Org. Chem.* 77, 9784-9794, (2012).
- 52. Mitchell, R. H. Conformational Changes of 2,11-Dithia[3.3]metacyclophane. A New Look Using VT NMR and Calculation. *J. Am. Chem. Soc.* **124**, 2352-2357, (2002).
- 53. Sauriol-Lord, F. & St-Jacques, M. Stereodynamic Investigation of Dibenzo-1,5-cyclooctadiene and 5,6,11,12-tetrahydrodibenzo[b,f] [1,4]diazocine Derivatives. *Can. J. Chem.* **53**, 3768-3776, (1975).
- 54. Montecalvo, D., St. Jacques, M. & Wasylishen, R. Direct Observation of Chair and Boat

- Conformations for Dibenzocycloocta-1,5-Diene by Nuclear Magnetic Resonance. *J. Am. Chem. Soc.* **95**, 2023-2024, (1973).
- 55. Nishimura, N. *et al.* Thermal Cis-to-Trans Isomerization of Substituted Azobenzenes .2. Substituent and Solvent Effects. *Bull. Chem. Soc. Jpn.* **49**, 1381-1387, (1976).
- Joshi, N. K., Fuyuki, M. & Wada, A. Polarity Controlled Reaction Path and Kinetics of Thermal Cis-to-Trans Isomerization of 4-Aminoazobenzene. *J. Phys. Chem. B* 118, 1891-1899, (2014).
- 57. Brown, E. V. & Granneman, G. R. Cis-trans isomerism in the pyridyl analogs of azobenzene. Kinetic and molecular orbital analysis. *J. Am. Chem. Soc.* **97**, 621-627, (1975).
- 58. Dokić, J. *et al.* Quantum Chemical Investigation of Thermal Cis-to-Trans Isomerization of Azobenzene Derivatives: Substituent Effects, Solvent Effects, and Comparison to Experimental Data. *J. Phys. Chem. A* **113**, 6763-6773, (2009).
- Norio, N., Shinya, K. & Yoshimi, S. The Thermal Isomerization of Azobenzenes. III. Substituent, Solvent, and Pressure Effects on the Thermal Isomerization of Push-pull Azobenzenes. *Bull. Chem. Soc. Jpn.* 57, 1617-1625, (1984).
- 60. Liu, L. & Guo, Q.-X. Isokinetic Relationship, Isoequilibrium Relationship, and Enthalpy–Entropy Compensation. *Chem. Rev.* **101**, 673-696, (2001).
- 61. Domiano, P. *et al.* The molecular structure of 6, 8, 6 and related systems. *J. Chem. Soc.-Perkin Trans.* 2, 1609-1620, (1992).
- 62. Gaussian 09 Revision E.01 (Gaussian, Inc: Wallingford, CT, 2016).

## **Table of Content only:**

# Tailored Conformational Changes of Dibenzocycloocta-1,5-dienes by Arene Substituent Effects for Controlled Switching

Wenxin Fu<sup>1</sup>, Jiachen Li<sup>3</sup>, Jacqueline Bustamante<sup>1</sup>, Thanh Lien<sup>4</sup>, Ralph W. Adams<sup>5</sup>, Simon J. Teat<sup>6</sup>, Benjamin J. Stokes<sup>4</sup>, Todd M. Alam<sup>7</sup>, Weitao Yang<sup>3</sup>, Yi Liu<sup>2</sup>, Jennifer Q. Lu<sup>1,\*</sup>

